RPC-MAG
The Fluxgate Magnetometer in the ROSETTA Plasma Consortium

KARL-HEINZ GLASSMEIER[1,*], INGO RICHTER[2], ANDREA DIEDRICH[2],
GÜNTER MUSMANN[2], ULI AUSTER[2], UWE MOTSCHMANN[2],
ANDRE BALOGH[3], CHRIS CARR[3], EMANUELE CUPIDO[3], ANDREW COATES[4],
MARTIN ROTHER[5], KONRAD SCHWINGENSCHUH[6], KAROLY SZEGÖ[7] and
BRUCE TSURUTANI[8]

[1]*Institut für Geophysik und extraterrestrische Physik, Technische Universität Braunschweig,
Mendelssohnstrasse 3, D-38106 Braunschweig, Germany*
[2]*Technische Universität zu Braunschweig*
[3]*Imperial College London*
[4]*Mullard Space Science Laboratory at Holmbury St. Mary*
[5]*GeoForschungsZentrum Potsdam*
[6]*Institut für Weltraumforschung Graz*
[7]*KFKI Reserach Institute for Particle and Nuclear Physics Budapest*
[8]*Jet Propulsion Laboratory Pasadena*
(*Author for correspondence: E-mail: kh.glassmeier@tu-braunschweig.de)

Abstract. The fluxgate magnetometer experiment onboard the ROSETTA spacecraft aims to measure the magnetic field in the interaction region of the solar wind plasma with comet 67P/Churyumov-Gerasimenko. It consists of a system of two ultra light (about 28 g each) triaxial fluxgate magnetometer sensors, mounted on the 1.5 m long spacecraft boom. The measurement range of each sensor is ±16384 nT with quantization steps of 31 pT. The magnetometer sensors are operated with a time resolution of up to 0.05 s, corresponding to a bandwidth of 0–10 Hz. This performance of the RPC-MAG sensors allows detailed analyses of magnetic field variations in the cometary environment. RPC-MAG furthermore is designed to study possible remnant magnetic fields of the nucleus, measurements which will be done in close cooperation with the ROSETTA lander magnetometer experiment ROMAP.

Keywords: comet, solar wind, plasma, fluxgate magnetometer, ROSETTA

1. Scientific Objectives

The objective of the fluxgate magnetometer experiment in the ROSETTA Plasma Consortium (RPC; see also Trotignon *et al.*, 1999) is to study the interaction of the magnetized solar wind plasma with comet 67P/Churyumov-Gerasimenko during its approach to the Sun, that means to study the evolution of the interaction region during increasing cometary activity. Two basically different modes of this interaction may be discriminated: interaction of the inactive cometary nucleus versus interaction of the active nucleus with the magnetized interplanetary medium.

© Springer 2007

The latter case has already been studied by previous spacecraft missions to comets 21P/Giacobini-Zinner (e.g. Tsurutani and Smith, 1986), 1P/Halley (e.g. Neubauer *et al.*, 1986; Yumoto *et al.*, 1986), 26P/Grigg-Skjellerup (e.g. Glassmeier and Neubauer, 1993), and 19P/Borrelly (Richter *et al.*, 2007). Cometary neutral gas is initially expanding from the nucleus with speeds as low as 1 km/s. EUV radiation from the Sun and hot electrons of solar wind origin ionize these neutrals. The newborn ions are subsequently picked-up by the electromagnetic field of the solar wind plasma. This mass loading causes a deceleration of the flowing solar wind, as already studied in detail by Biermann *et al.* (1967). As the solar wind is a supersonic flow cometary ion pick-up eventually leads to the formation of a weak shock in front of the comet. Behind this shock the solar wind plasma is deflected around the obstacle, the outgassing cometary nucleus. As plasma flow and interplanetary magnetic field are closely coupled the magnetic field is draped around the nucleus, a picture already conjectured by Alfvén (1957). Comet-solar wind interaction is thus a particularly interesting case of the physics of mass-loaded plasmas (e.g. Szegö *et al.*, 2000).

This classical picture of the comet-solar wind interaction has been confirmed by flybys at comets 21P/Giacobini-Zinner, 1P/Halley, 26P/Grigg- Skjellerup, and 19P/Borelly. However, major aspects of the interaction need further detailed consideration. First, the temporal evolution of the interaction needs to be studied. With increasing activity the type of interaction will change. Presently only numerical simulations are available to study this evolution (e.g. Bagdonat *et al.*, 2004). Second, the formation of a cometary magnetic cavity (e.g. Neubauer, 1987) is a process which deserves further experimental study. Third, cometary tail disruptions are processes not understood yet. Fourth, the microphysics of the generation and evolution of large amplitude low-frequency waves and turbulence in the interaction region (e.g. Glassmeier *et al.*, 1997) needs further attention as these waves serve to isotropize and thermalize the newborn pick-up ions of cometary origin and thus are of paramount importance in the cometary mass loading process.

Figure 1 displays observations of the magnetic field magnitude made during the flybys at comets 1P/Halley, 26P/Grigg-Skjellerup, 21P/Giacobini-Zinner, and 19P/Borrelly. As the flyby trajectories and velocities are different, several scalings have been applied to the data to allow a comparison.

The flyby velocity at 1P/Halley was much larger than at 26P/Grigg-Skjellerup, 21P/Giacobini-Zinner, and 19P/Borelly, 68.7 km/s vs. 14.0, 20.7, 16.6 km/s, respectively. This causes a much higher spatial resolution of plasma properties at the latter three comets. Thus, the resolution has been adapted to that achievable at 1P/Halley by using data appropriately averaged. The s/c trajectories at 1P/Halley and 26P/Grigg-Skjellerup are very similar in that the s/c passed by the comets on the nucleus' dayside, while at 21P/Giacobini-Zinner the tail has been traversed. At 1P/Halley the s/c passes from the afternoon side towards early morning and at 26P/Grigg-Skjellerup in the reverse direction. We take into account this difference by inverting the time axis for the 26P/Grigg-Skjellerup data. The DEEP SPACE-1
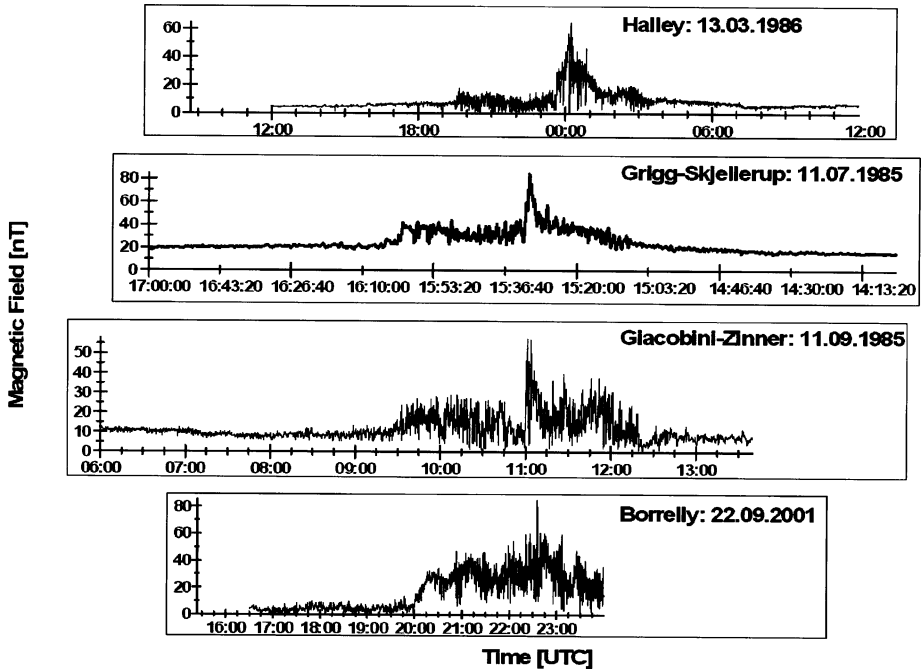
Figure 1. Magnetic field observations made during the flybys at comets 1P/Halley, 26P/Grigg-Skjellerup, 21P/Giacobini-Zinner, and 19P/Borrelly.

spacecraft passed 19P/Borelly at a closest approach distance of 2172 km in the upstream region of the comet. Furthermore, the different macroscopic scales have been taken into account by selecting time periods displayed such that the data coincide at the bow shock locations.

Inspection of Figure 1 allows one to conclude that the macroscopic features of the interaction regions are very similar. Especially, the similarities between 1P/Halley and 26P/Grigg-Skjellerup are striking. At 1P/Halley, in front of the inbound bow shock the magnetic field magnitude is slowly increasing due to increasing mass loading (e.g. Neubauer, 1991) with a major increase occurring at the bow shock itself. In the cometary magnetosheath, the magnetic field magnitude decreases again with another rise occurring close to the pile-up boundary. The outbound profile, i.e. the early morning profile, is different in that the magnetosheath decrease of the field magnitude is not as pronounced as on the afternoon side. Furthermore, a long steady ramp of magnitude variations is detectable. Similar features are also observed at the other comets.

Additional differences are related to the plasma waves generated by the pick-up process. At 1P/Halley with its large gas production rate the interaction region with the solar wind is much larger than at the other comets visited hitherto. As a consequence any large-amplitude waves decayed into well developed plasma turbulence.

On the other hand, at comet 26P/Grigg-Skjellerup with its much smaller production rate ion pick-up generated waves kept their very nature and were observed as large-amplitude non-linear wave events. Comet 67P/Churyumov-Gerasimenko approaching the Sun will go through different phases of activity with the different phases resembling comets with different activity levels. Approaching the Sun together with the comet the ROSETTA spacecraft is conducting a journey in parameter space (e.g. Glassmeier *et al.*, 1997).

These phenomenological similarities and differences detected in the various cometary interaction regions already allow insights into the evolution of the cometary interaction with increasing cometary activity, as all four comets, 21P/Giacobini-Zinner, 1P/Halley, 26P/Grigg-Skjellerup, and 19P/Borelly exhibit very different neutral gas production rates. However, the ROSETTA plasma instruments and RPC-MAG will allow a much more detailed study of these differences, as the same object is studied under different activity levels.

Other aspects of the global interaction picture which require further attention are cometary plasma tail formation processes and cometary tail dynamics with spectacular features such as tail rays (e.g. Ness and Donn, 1966) or tail disconnection events (e.g. Niedner and Brandt, 1978). Though the ICE s/c traversed the tail of 21P/Giacobini-Zinner at a distance of about 10,000 km from the nucleus (Smith *et al.*, 1986) not much information about the tail forming processes resulted. Also, the detailed plasma physical processes leading to tail rays or initiating disconnection events are awaiting further *in-situ* observations to which RPC-MAG can contribute. This area of research also offers a unique possibility for coordinated ground-based observations and *in-situ* measurements as demonstrated by e.g. Slavin *et al.* (1986). In particular, a tail excursion of the ROSETTA s/c would offer the possibility to study the tail formation region on the nightside, tail rays, and disconnection events in a hitherto unprecedented way.

The other mode of interaction is that of the interaction of the solar wind with the inactive nucleus. Not much is known about this type of interaction. It may be of a lunar type, where the solar wind is directly impinging on the surface and subsequently absorbed. Or the interaction is more like the interaction with a magnetized asteroid such as 951Gaspra and 243Ida (e.g. Kivelson *et al.*, 1993; Baumgärtel *et al.*, 1994; Blanco-Cano *et al.*, 2003; Simon *et al.*, 2006). Furthermore, the interaction very much depends on the electrical properties of the comet. There are two means of determining the electrical conductivity of the cometary nucleus by studying the solar wind interaction. One is the search for unipolar induction and associated effects, that is to search for magnetic field signatures driven by electric currents in the nucleus due to the solar wind interaction (e.g. Russell and Huddleston, 2000). The other is to search for the induction effects of time-varying solar wind magnetic fields (e.g. Sonett and Colburn, 1968). If the electrical conductivity of the cometary nucleus is small unipolar induction effects are negligible. The interplanetary magnetic field will pass through the nucleus with only little disturbance or draping. However, if the conductivity is larger than the Alfvén wave conductivity of the

RPC-MAG measurement requirements

Parameter	Value
Range	±16384 nT
Quantization	20 bit; 31 pT
Sampling rate	20 vectors/s
Bandwidth	0–10 Hz

solar wind plasma, significant changes of the interplanetary magnetic field are expected. Provided ROSETTA approaches the nucleus during such a low-activity period RPC-MAG may be able to determine the electrical properties of the nucleus.

Due to the small size of the nucleus as well as its internal structure no magnetic dynamo process is expected to operate in a cometary nucleus. Any cometary magnetic field must be either due to induction by the solar wind interaction or due to remnant magnetization of the nucleus material. Nübold and Glassmeier (1999), for example, studied accretional magnetization of magnetized interplanetary dust particles. They have been able to demonstrate that clusters of up to about 100 magnetic dust particles can form, still exhibiting a net magnetic moment. Whether larger magnetized objects during comet nucleus formation can be built is not yet known. However, in close cooperation with the ROSETTA lander magnetometer ROMAP (Auster *et al.*, this issue) the magnetic properties of the nucleus will be studied during the descent of the lander.

These are only some of the interesting scientific questions which will be addressable using future observations of RPC-MAG and the other sensors of the ROSETTA Plasma Consortium. The measurement requirements for the magnetometer to achieve its scientific goals are described in the ROSETTA Experiment Interface Control Document (EID-B) and given in Table I.

2. Instrument Description

To achieve the scientific objectives described above two ultralight triaxial fluxgate magnetometer sensors were mounted close to the tip of the 1.5 m long spacecraft boom and 15 cm closer to the s/c on the same boom (see also Figure 2 of Carr *et al.*, this issue). Two magnetometer sensors are required to determine the influence of the rather complex spacecraft magnetic field on the actual measurements, and for redundancy purposes.

The heritage of the ROSETTA orbiter magnetometer goes back to spacecraft missions such as the solar wind missions HELIOS A/B (Musmann *et al.*, 1975), GIOTTO (Neubauer *et al.*, 1985), CLUSTER (Balogh *et al.*, 1993), and DEEP SPACE 1 (Richter *et al.*, 2001). The sensor actually used on the ROSETTA orbiter
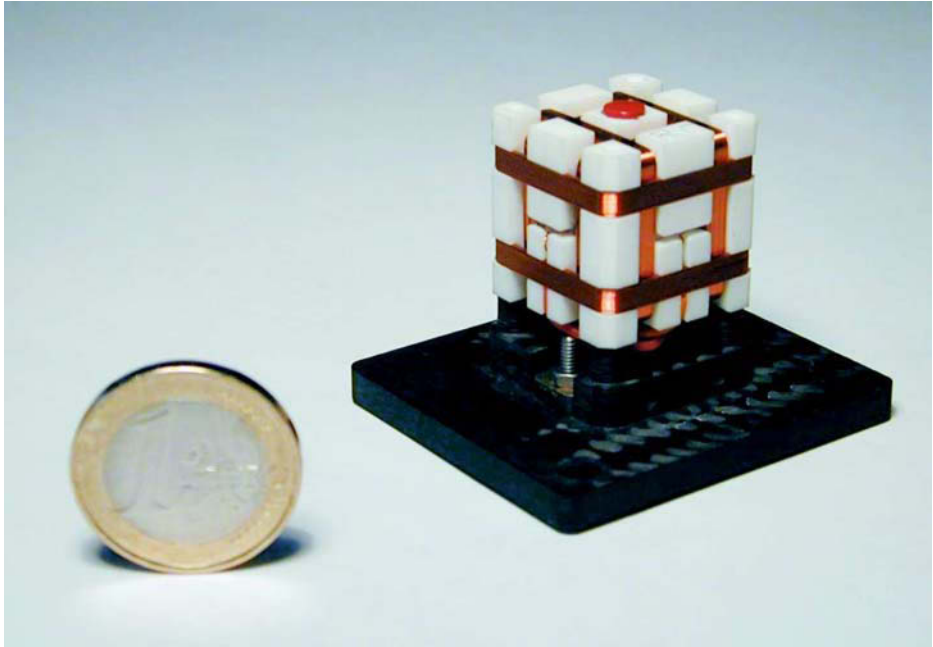
Figure 2. The RPC-MAG fluxgate sensor.

is a flight-proven sensor: in its basic configuration it has been used on NASA's
DEEP SPACE 1 mission.

This ROSETTA orbiter double-ring core MACOR-cube fluxgate sensor has
dimensions of about $25 \times 25 \times 25$ mm^3 and a mass of 28 g (see Figure 2). As
in all fluxgate magnetometers, a ferromagnetic core of soft magnetic material is
periodically driven into saturation by the magnetic field of a drive coil. In case of
ROSETTA RPC-MAG the drive coil frequency is $f_D = 12.5$ kHz. The core used
is a very low noise double-ring core of molybdenum permalloy. In addition to
the drive coil three pick-up coils take the magnetized field, which exhibits second
harmonics at $2 f_D$ in the presence of any ambient magnetizing field. The magnitude
of this second harmonic is proportional to the ambient magnetic field strength. The
pick-up coils form a triaxial Helmholtz coil system with the double-ring core in
its center. This helps to avoid cross-talk between sensor components and nonlinear
sensor sensitivity.

The pick-up signal is digitized by a 20 bit A/D converter. To increase time
resolution six ADCs are used, one for each of the six (two times three sensor axes)
sensor channels. A seventh ADC is used for house-keeping channels of the other
RPC instruments.

RPC-MAG is operated with a time resolution of 20 vectors/s outboard and 1
vector/s inboard, e.g. the bandwidth is 10 Hz and 0.5 Hz, respectively. The actual
number of vectors delivered to the s/c telemetry depends on the available telemetry
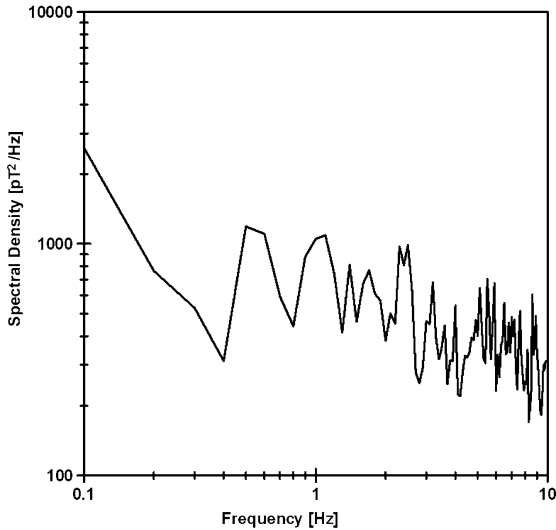
Figure 3. Noise spectrum of a typical RPC-MAG fluxgate sensor component.

rate and is adopted by averaging of the vector rate inside the RPC-PIU (see Carr *et al.*, this issue).

RPC-MAG has only a single measurement range, ±16384 nT, in order to decrease the complexity of instrument operations. With a 20 bit ADC this results in quantization steps of 31 pT, which is well above our typical analog sensor noise. Figure 3 displays the noise spectrum of a typical sensor axis in the frequency range 0.1–10 Hz. The spectrum has been determined analyzing the analog signal from the sensor, shielded by a permalloy can. The maximum noise spectral density is of the order of 22 pT/$\sqrt{Hz}$, which corresponds to a total r.m.s. noise level of about 22 pT.

The RPC-MAG block diagram is displayed in Figure 4 and shows that the digitized sensor output is controlled via a field programmable gate array (FPGA), which also handles the sampling of all six channels and also provides the connection to the RPC-PIU interface (see Carr *et al.*, this issue). The ADC part was developed and provided by the Institute of Space Research (IWF) in Graz, the analog electronics and the FPGA as well as the sensors were developed and provided by the Institute of Geophysics and extraterrestrial Physics (IGeP) in Braunschweig. The Experiment Ground Support Equipment was provided by the co-investigator group at Imperial College supported by the KFKI group in Budapest, where also the FPGA programming was done. Instrument management is the responsibility of IGeP.

3. The Magnetic Cleanliness Program

A reduced magnetic cleanliness program was carried out in the course of the ROSETTA project. The prime responsibility of this magnetic cleanliness program
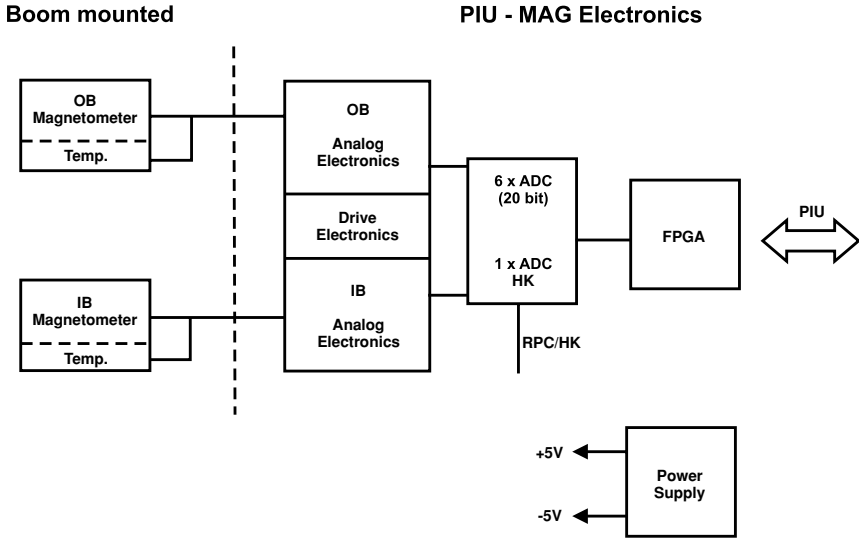
Boom mounted   **PIU - MAG Electronics**

Figure 4. The RPC-MAG block diagram. The sensors are boom mounted and connected to the Plasma Interface Unit (PIU) via the sensor analog electronics.

was shared between EADS Astrium in Friedrichshafen, IGeP in Braunschweig, and ESA's European Space Research and Technology Centre (ESTEC) in Noordwijk. For all spacecraft subsystems and experiments, the maximum allowed magnetic field at the position of the outboard magnetometer sensor was limited to 25 nT.

Three major sources of spacecraft magnetic fields are important: hard magnetic material, causing a permanent magnetic field at the sensor location, soft magnetic materials, giving rise to time varying magnetic fields due to changing background field conditions, and currents drawn by active parts onboard or devices such as the solar panels and motors.

Basic principles of the magnetic cleanliness programme are: identification and magnetic mapping of all critical units of the engineering model, modelling all units using ESA's GANEW software based on procedures first introduced by Mehlem (1978), mapping of flight model units and compensation as necessary, and magnetic mapping using the IGeP developed mobile coil system at the flight model integration site. This procedure helped to minimize contributions from hard magnetic materials and to identify soft magnetic parts. For example, thrusters carry a magnetic moment of about $500\,\mathrm{mAm}^2$, while the magnetic influence of e.g. the solar panels can be minimized by a dedicated backwiring scheme to less than 1 nT at the outboard sensor.

A reduced final system magnetic test and compensation as necessary was done at ESTEC. A dedicated PHILAE lander magnetic cleanliness programme was carried out using the Magnetfeldsimulationsanlage (MFSA) of the IABG GmbH in Ottobrunn with similar activities (e.g Kügler, 2004a). The DC stray field based on checking over 80 spacecraft units are at the locations of the inboard and outboard

sensor, respectively, 48 nT and 33 nT. This is close to the specified values of 25 nT. Contributions from the thrusters, the solar array drive mechanism, the lander, and ROSETTA's navigation camera were largest.

4. Sensor Calibration

The ground calibration of the RPC-MAG sensors has been conducted at the Technical University of Braunschweig in the 2.5 m three axes Braunbek coil system (Braunbek, 1934) at the premises of the MAGNETSRODE calibration laboratory of IGeP (Kertz *et al.*, 1968; Lühr, 1980; Kügler, 2004b). The coil system (Figure 5) consists of 12 coils, i.e. four coils for each of the three orthogonal axes. Each coil contains current carrying windings for geomagnetic field compensation, static and dynamic magnetic field generation, diurnal variation control, etc. Artificial DC and low-frequency AC magnetic fields of up to 100,000 nT can be generated in this coil system. This allows an active compensation of the local geomagnetic field as well as the application of an artificial field representing the geomagnetic field at every point of the Earth' surface and near-Earth interplanetary space.

The calibration procedure follows previous successful calibrations for the GIOTTO, AMPTE, CLUSTER, CASSINI, EQUATOR-S, DEEP SPACE 1, THEMIS, and VENUS EXPRESS spacecraft. The following parameters were calibrated: linearity, sensitivity, sensor misalignment, offsets, frequency response, crosstalk between sensor components, and temperature drift of the sensors between $-80\,°C$ and $+80\,°C$. Functional tests have been executed down to temperatures of $-160\,°C$, the minimum expected temperature on the ROSETTA magnetometer boom.

For calibration of the linearity, sensitivity, misalignment, and crosstalk field vectors homogeneously distributed inside a sphere were applied to the sensors via the Braunbek coil system. During calibration the external magnetic field was compensated via continuous monitoring with the Magnetsrode Station Magnetometer down to ± 0.8 nT.

The calibration method applied is as follows (e.g. Kügler, 2004b). The real, calibrated, and applied magnetic field vector $\mathbf{B}_{cal}$ is given by

$$\mathbf{B}_{cal} = \mathcal{S}_c \circ \mathcal{A} \cdot \mathbf{U}_{sol}, \tag{1}$$

where $\mathbf{U}_{sol}$, $\mathcal{S}_c$, and $\mathcal{A}$ are the requested field vector measured with a Solartron voltmeter, the temperature dependent Braunbek coil system sensitivity matrix, and the coil system alignment matrix, respectively. The relation between the applied calibrated field vector $\mathbf{B}_{cal}$ and the field measured by the sensor to be calibrated, $\mathbf{B}_{mea}$, is given by

$$\mathbf{B}_{mea} = \mathcal{M} \cdot \mathbf{B}_{cal} \tag{2}$$
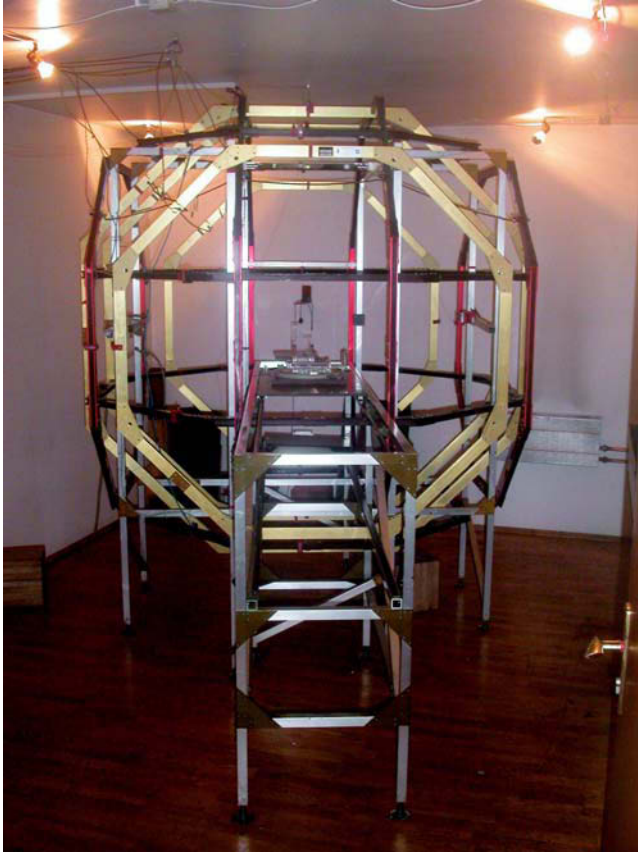
Figure 5. The Magnetsrode Braunbek Coil System of the Technical University at Braunschweig.

with

$$\mathbf{B}_{\mathrm{mea}} = \mathcal{G} \cdot \mathbf{U}_{\mathrm{exp}}, \tag{3}$$

where $\mathcal{M}$, $\mathcal{G}$, and $\mathbf{U}_{\mathrm{exp}}$ are the calibration matrix to be determined, the matrix transforming voltages into magnetic field values, and the output voltage vector of the sensor, respectively. The aim of the calibration procedure is the determination of the matrix $\mathcal{M}$ from known and measured values of $\mathbf{B}_{\mathrm{cal}}$ and $\mathbf{B}_{\mathrm{mea}}$.

The calibration matrix $\mathcal{M}$ can be represented as a product of three matrices according to

$$\mathcal{M} = \mathcal{S} \circ \mathcal{O} \circ \mathcal{R}, \tag{4}$$

where $\mathcal{R}$ is the rotation matrix describing the orientation of the sensor triple in the coil system, $\mathcal{O}$ is the temperature dependent orthogonalization matrix describing the sensor misalignment, and $\mathcal{S}$ is the sensitivity matrix. The misalignment corrected sensitivity matrix has only three non-zero diagonal coefficients, the rotation matrix is described by its three Euler angles, and the orthogonalization matrix

$\mathcal{O}$ is determined by three independent misalignment angles only. Thus, from the nine independent, temperature dependent coefficients of the matrix $\mathcal{M}$ the three other matrices $\mathcal{R}$, $\mathcal{O}$ and $\mathcal{S}$ can be determined. Sensor offsets are determined by applying null-fields and rotating the sensor by $\pm 180\,°$.

Using this calibration algorithm and the MAGNETSRODE calibration facility the following results were obtained: accuracy of sensor sensitivities $\pm 10^{-5}$, temperature coefficients of the sensitivities $-10^{-5} \mathrm{K}^{-1}$, misalignment angle better than ± 1 arcmin, temperature dependence of these angles about $5 \cdot 10^{-3}$ arcmin K^{-1}, offsets at fixed temperatures about ± 0.8 nT, temperature dependence of the offsets about $\pm 1\, \mathrm{nT\,K}^{-1}$. These later temperature coefficients vary by about $\pm 0.5\, \mathrm{nT\,K}^{-1}$ for different temperature cycles as the sensor core material exhibits hysteretic behavior.

Furthermore, the influence of the sensor electronic temperature has been checked during ground tests. They reveal that there is no noticeable impact of the electronics temperature in its operating range of $25\,°$–$35\,°$ on the magnetic readings. Therefore the sensor electronics temperature is not taken into account during data analysis.

5. Commissioning Results

The commissioning campaign for RPC-MAG was divided in four parts. The first commissioning and verification phase (CVP1) was executed in the time interval March 17–19, 2004, the second phase (CVP2) during May 5–10, 2004, and the third test period (CVP3) was carried out during September 6–10, 2004. A final test, the interference campaign, was done between September 20 and October 14, 2004. The most exciting phase, however, was CVP1, when RPC-MAG was switched on for the first time in space at 22:57 UTC on March 17, 2004. The experiment was checked out successfully in the housekeeping mode and all five science modes. Data were measured with both, the inboard sensor and the outboard sensor. All systems worked flawlessly to expectation. The boom temperatures during CVP1 varied in a wide range between about $-100\,°$C and $-60\,°$C.

The really crucial phase of the commissioning took place in the early morning of March 18, 2004, when the magnetometer boom was deployed. Explosive charges, the pyros, were fired to release the boom from its stowed position at 03:36 UTC and five minutes later the boom was completely deployed. The magnetic signature of this event is displayed in Figure 6 using instrument coordinates. In its stowed position the boom was pointing almost along the -y-direction of the spacecraft coordinate system, mounted on the rear side of the spacecraft, that is the y-z plane where the ROSETTA lander PHILAE is mounted. In its deployed state it is constructed to point almost along the negative x-direction of the ROSETTA spacecraft system. This rotation was documented by the magnetometer and is clearly identifiable in Figure 6, where the change of the magnetic field in all three components is visible. The small overshoot at about 03:37 UTC indicates a short boom oscillation. The
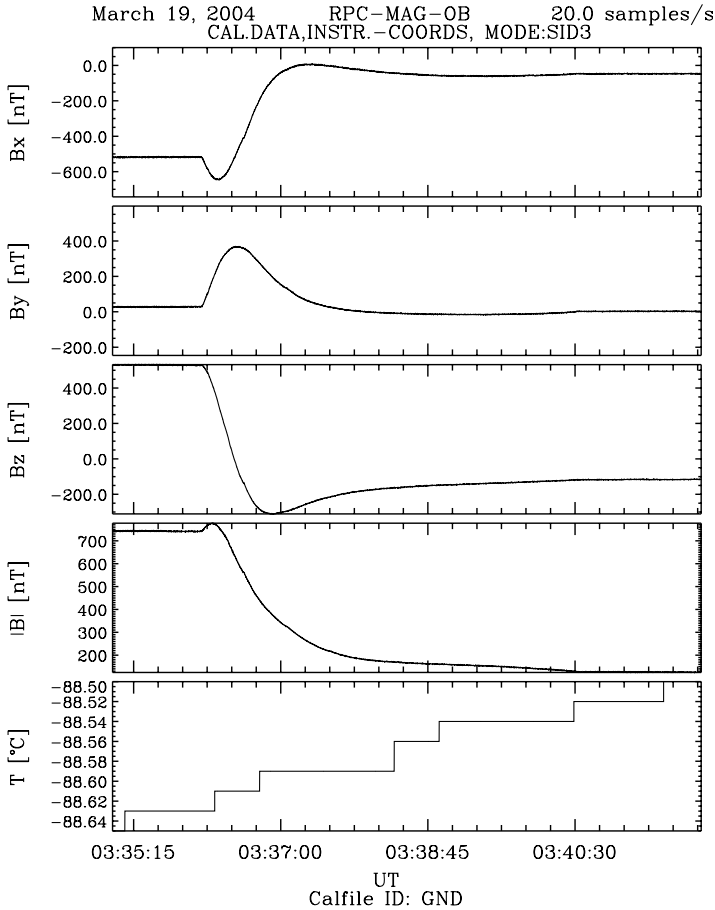
Figure 6. Magnetic field measurements, in instrument coordinates, made by the outboard sensor during boom deployment.

deployment also reveals that the residual magnetic field magnitude of is about 740 nT at the location of the outboard sensor in the stowed position and about 100 nT in the deployed position. Furthermore, the noise level after boom deployment was about a factor of ten lower than before the deployment. The sensor temperature during the deployment was constant at about $T = -88\,°C$.

During the remaining commissioning phases the RPC-MAG sensors were operated in the temperature range $-125\,°C$ to $-45\,°C$. This provided for a suitable opportunity to extend the determination of the temperature dependent calibration matrix. From ground calibration it is known that the sensitivity, the sensor misalignment, and the sensor offsets are temperature dependent. This dependency could, however, only be determined down to $-80\,°C$ during the ground calibration due to facility limitations. Taking into account all measurements made during the commissioning
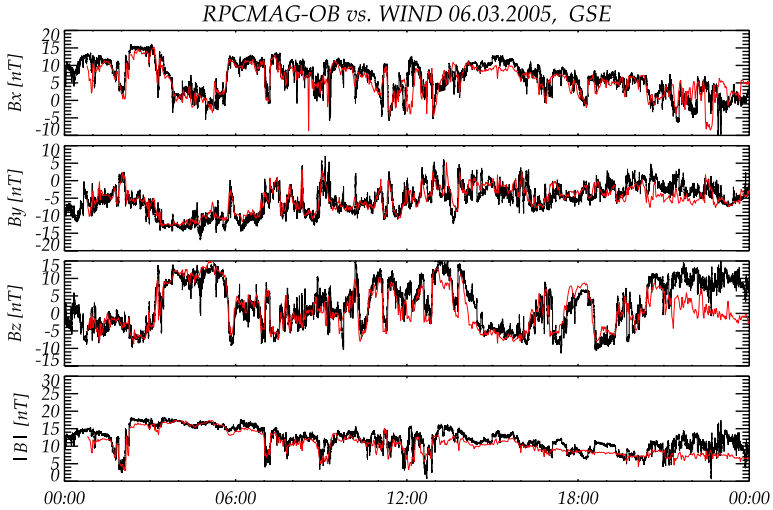
Figure 7. Comparing RPC-MAG and WIND. The data are represented in geocentric solar ecliptic (GSE) coordinates. The black line represents the RPC-MAG measurements.

phases and using 10 min averaged data an improved third order polynomial temperature model could be developed down to temperatures at $-125\,°C$. Especially sensor offset determination has been significantly improved in this way. The new temperature model was tested comparing solar wind magnetic field measurements made during ROSETTA's first Earth flyby and WIND magnetic field data. During the Earth flyby the WIND spacecraft was located about 238 Earth radii towards the Sun. The WIND magnetic field observations have thus been time shifted by 47 min with respect to those made onboard ROSETTA (Figure 7). The agreement between both data sets is striking and confirms the quality of the temperature model developed.

In addition to the analysis of normal mode RPC-MAG data in the low-frequency range an analysis of burst mode data at higher frequencies has been performed. Dynamic spectra reveal the continuous presence of a sinusoidal disturbance of the order of 1 nT peak-to-peak with the frequency slowly changing in time (Figure 8). This disturbance can be seen on both, the inboard and outboard sensor as well as in measurements made by the lander magnetometer ROMAP (Auster *et al.*, this issue). The frequencies of this observed disturbance are different for different sampling modes. This led to the hypothesis that this interference is due to ROSETTA's four reaction wheels and aliasing effects causing the dependence of the disturbing signal on sampling modes.

To test this hypothesis and to understand how the higher frequency reaction wheel speeds can be seen by the RPC-MAG magnetic sensor sampled at 20 Hz (burst mode) or 1 Hz (normal mode) the possible influence of the reaction wheels has been modelled using reaction wheel frequency data from ROSETTA's Data Distribution System (DDS). After shifting and folding the wheel data down to the
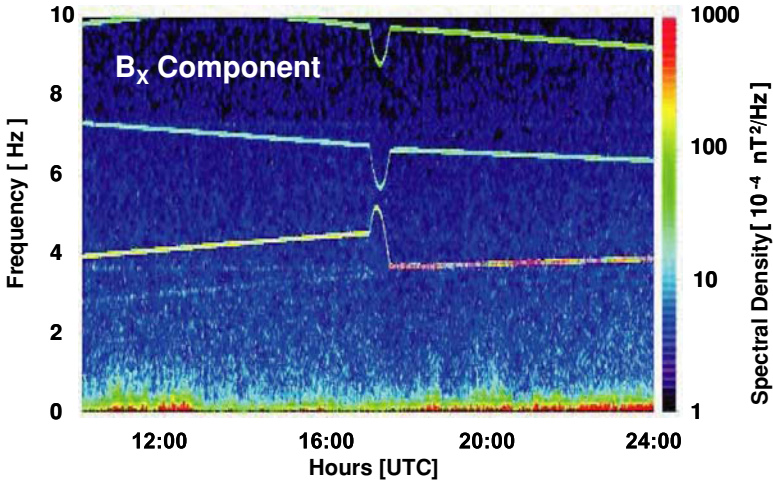
Figure 8. A typical dynamic spectrum of outboard sensor measurements in burst mode (20 Hz sampling frequency) made on September 9, 2004. Spacecraft coordinates are used.

Nyqvist frequency using the sampling theorem the modelled and measured spectra reveal a striking similarity confirming the reaction wheel as the disturber looking for. As a spin-off the analysis of RPC-MAG outboard and inboard sensor data as well as independently determined ROMAP measurements provided for a slightly improved determination of the reaction wheel frequency. The nominal values were 1360–1820 rpm. They had to be corrected by a factor 1.00335, corresponding to a correction of about 4 rpm.

As the ROSETTA lander, PHILAE, also carries a fluxgate magnetometer, ROMAP (Auster *et al.*, this issue), a detailed comparison between all three sensors, the RPC-MAG inboard and outboard sensors and the ROMAP sensor is possible. Figure 9 displays corrected magnetic field variations as seen by all three sensors during the early phase of ROSETTA's first Earth flyby. Despite offset differences all three records agree very well with each other.

Based on these commissioning results RPC-MAG has been qualified as a well working two-sensors fluxgate magnetometer system. Temperature effects can be corrected using the improved temperature calibration model. Interference at higher frequencies such as the reaction wheels have been identified and suitable software to eliminate them has been developed.

6. Data Processing and Reduction

The magnetic field data measured by the outboard and inboard sensors are downlinked as 20 bit ADC voltage values. As a first processing step these signals are converted into non-calibrated DC magnetic field values using the nominal
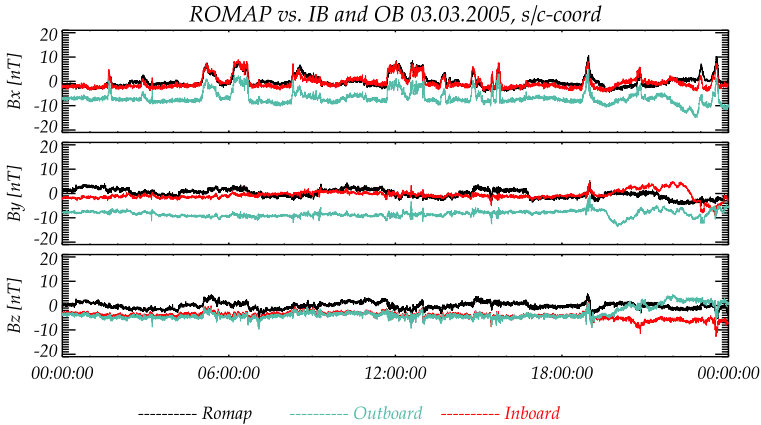
Figure 9. Magnetic field measurements of all three ROSETTA magnetometer sensors during the early Earth flyby phase.

ADC-digits-to-voltage procedure and a coarse linear scaling to obtain engineering nT-values. As a result so called edited raw data are generated. As a second step any corrupted data vectors are discarded and ground calibration results such as sensitivities, sensor misalignment matrices, and instrument offsets are applied to these edited raw data. It is worth mentioning that all these calibration parameters are temperature dependent. Therefore, the calibration has to be applied vector by vector using the actual sensor temperatures stored in the instrument housekeeping frames.

To have comparable data sets both, the magnetic field vectors from the inboard and outboard sensors are rotated from their respective sensor frame of reference into the spacecraft coordinate system. At this step the first level of calibrated data are available. To obtain scientific usable data these calibrated vectors have to be rotated from the spacecraft coordinate system into a suitable celestial reference frame, e.g. ECLIPJ2000, GSM, GSE or whatever is convenient in the considered mission phase. This is done taking into account the spacecraft attitude at every point of time. This information is extracted from the spacecraft quaternion files produced by the European Space Operation Center (ESOC) flight dynamics team. The rotation into the desired celestial frame is preferably done using SPICE routines (Acton, 1996).

The further steps of the data processing depend on the actual spacecraft status and analysis requirements. As a minimal standard procedure the data can be averaged to a suitable mean. If, however, the impact of the spacecraft reaction wheels is visible in the magnetometer data (see above), which happens occasionally, an extensive elimination algorithm, operating in the frequency domain, can be applied. This algorithm calculates the dynamic frequency response of the four instantaneous reaction wheel frequencies with respect to the Nyqvist frequency of the actual magnetometer sampling rate. The necessary reaction wheel information is retrieved

from ancillary data files in the ROSETTA DDS. These frequency values are exactly the aliased spectral lines showing up in the dynamic spectra of the magnetometer measurements an example of which is displayed in Figure 8. Knowing the spectral location of these lines permits their elimination by suppressing the local spectral amplitude down to the weighted background values of the spectrum. A back transformation into the time domain reveals a purged time series without any signature of the reaction wheels.

A further special processing of the data is required if the heaters of the ROSETTA lander are operating. The magnetic field generated by the pulsed DC currents feeding these heaters is visible in the order of 1 nT peak-to-peak amplitude at the RPC-MAG sensors. Three heaters are operating with different discrete currents and a pulse width of the order of 30 s, causing multi-level signal signatures. The currents of the lander heater cannot be derived from the housekeeping data for several reasons. First, the principal temporal resolution of the housekeeping data packets is only 32 s, whereas the maximum sampling rate of the magnetometer is 20 Hz. Second, the only housekeeping value available is the total Lander current with a resolution of only a few mA. Third, there are several heaters whose individual currents are not tracked. The control software switches these heaters autonomously and does not generate any event packets reporting the actual heater status.

However, elimination of the heater signals can be achieved using a moving variance filter procedure. As a first step the time series of the disturbed magnetic field vectors is rotated into its minimum variance system. A maximum variance approach can be used here as the main magnetic disturbance is caused by the main current line, not by the individual lines at the positions of the heaters. This implies that only the magnitude of the disturbance changes, not its direction.

For every point in time a second step involves the determination of a short term moving average variance of the maximum variance component using, for example 10 samples. The time series derived in this way has to be compared with a suitable chosen constant threshold. Any variance value above the threshold denotes a jump caused by the heater currents. Once the times of the jumps have been identified the height of the jumps can be evaluated by computing short time interval averages before and after the jumps identified. In this way good and disturbed levels in the magnetic field measurements are identified and adjusted by shifting the disturbed levels to the undisturbed ones. Once this is done the time series needs to be resampled as the intermediate points during the transitions between the levels are lost. Finally, the resampled data have to be rotated back from the minimum variance system into the original coordinate system. The described procedure works for different time intervals, but still needs some further adjustment depending on the time interval processed. It should be noted that the above described procedure is only necessary as long as the lander is still connected to the ROSETTA orbiter.

During the nominal cometary phase with the lander disconnected only the standard data processing procedures need to be applied. In addition to the ground
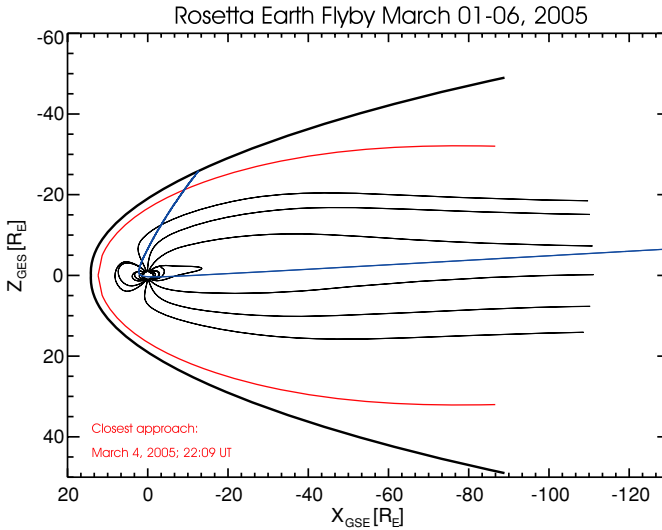
Figure 10. The ROSETTA trajectory during the first Earth flyby March 1–6, 2006. A model bow shock (thick black line) as well as a model magnetopause (red line) are also displayed.

calibration further inflight calibrations using procedures such as the Hedgecock technique (Hedgecock, 1975; Markgraf *et al.*, 1996) are necessary and supporting the calibration task. However, at the present time the application of these methods is not yet possible as no suitable data intervals are available.

7. First Earth Flyby Results

Launched on March 2, 2004 ROSETTA has to perform four planetary swingby manoeuvres on its way to 67P/Churyumov-Gerasimenko. The first one took place on March 4, 2005 with planet Earth. It was a unique swingby in many respects. ROSETTA entered the terrestrial magnetosphere in the distant tail flying all along the center of the tail for almost three days until closest approach which occurred on March 4, 2005, 22:09 UTC (Figure 10). The minimum distance to Earth was 1961 km, when ROSETTA passed over the Pacific Ocean just west of Mexico with a ground velocity of about 38 km/s (Figure 11).

RPC-MAG was switched on at 00:01 UTC on March 1, 2005 and provided continuous measurements with a sampling rate of 1 Hz until March 7, 23:41 UTC. Several different flyby phases can be identified (Figure 12): the tail phase, closest approach, outbound magnetopause crossing, magnetosheath traversal, outbound bow shock crossing, and the outbound solar wind phase. The flyby offered a unique possibility to gather a kind of snapshot of the Earth magnetosphere, especially the magnetotail, as solar wind conditions have been rather quiet during this first Earth swingby. A detailed scientific analysis of these flyby data is the subject of a separate
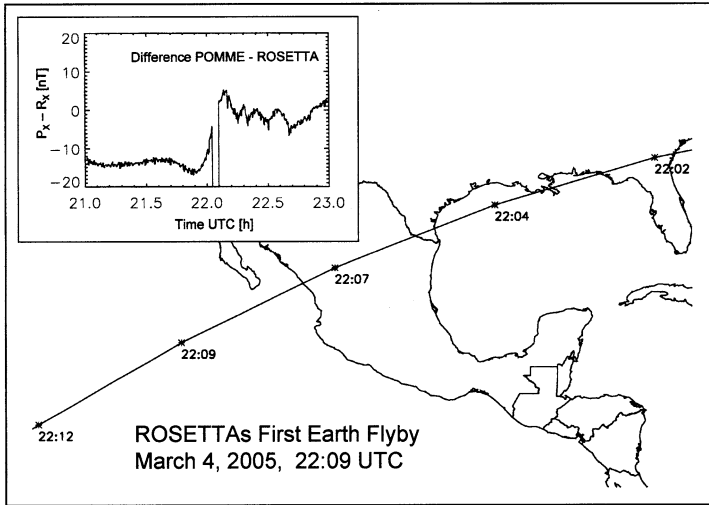
Figure 11. Ground track of ROSETTA around closest approach during its first Earth flyby. The insert displays the difference field in the GSE *x*-coordinate between the field modelled using POMME and the actually measured field onboard ROSETTA. P_X and R_X denote the *x*-component of the modelled and measured field, respectively. The maximum difference between measured and modelled field at 22:04 UTC is 220 nT.
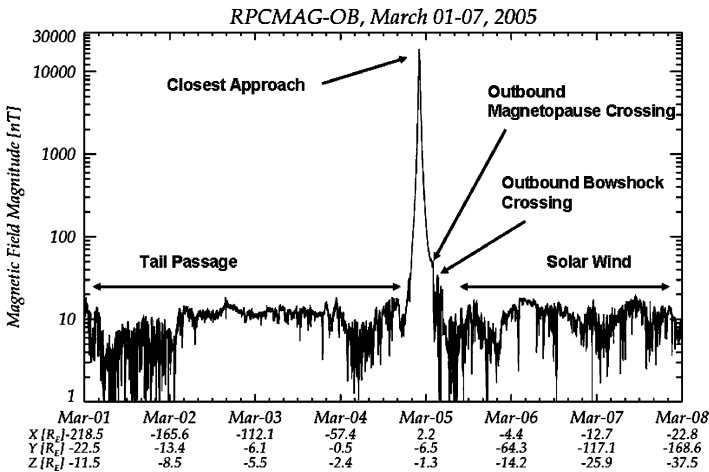

Figure 12. Magnitude of the magnetic field measurements made in the terrestrial magnetosphere during ROSETTA's first Earth flyby during March 1–7, 2005.

analysis (Glassmeier *et al.*, 2007). Here we use ROSETTA's Earth flyby as a very good opportunity to perform an inflight calibration of the RPC-MAG sensor.

The small flyby distance allows a detailed comparison with models of the geo-magnetic main field. Here we use the Potsdam Magnetic Field Model of the Earth

(POMME; see Maus and Rother (2004)). POMME is a main field model based on recent observations of the OERSTED and CHAMP spacecraft magnetic field missions (Olsen *et al*., 2000; Maus *et al*., 2002). It takes into account the time varying core field, the magnetospheric ring current, time averaged magnetospheric magnetic fields, and a crustal magnetic field model based on spherical harmonic analysis up to degree 90.

The maximum measured magnetic field magnitude at closest approach was 18,776 nT with maximum field values in the *x*-axis within the measurement range ±16,384 nT. At closest approach the POMME model predicts a magnetic field magnitude of 18,774 nT, provided the onboard time of the outboard sensor is corrected for a time shift of −8.37 s. For this time shift the agreement between the POMME predicted field and the measured field magnitude is optimized. This very good agreement in the field magnitude can be further improved when the measured data are rotated by (0.111 °, −0.054 °, 0.372 °) about the *x*-, *y*-, and *z*-axis. This difference between measured and modelled field is then reduced to about 20 nT in the field components. From this we conclude that the sensor alignment is not exactly as determined by ground measurements.

A detailed comparison is displayed in the insert of Figure 11. The large difference at 22:04 UTC is as yet unexplained. It occurred during ROSETTA passing over the city of New Orleans at a height of 2310 km. The difference vector points roughly NNW and about 60 ° down. This difference cannot be understood as a spacecraft signature. Most probably it is due to some local ionospheric current system which is not modelled by the POMME main field model.

As a further example Figure 13 displays high-resolution data taken during ROSETTA's outbound magnetopause crossing. In the spacecraft frame of reference
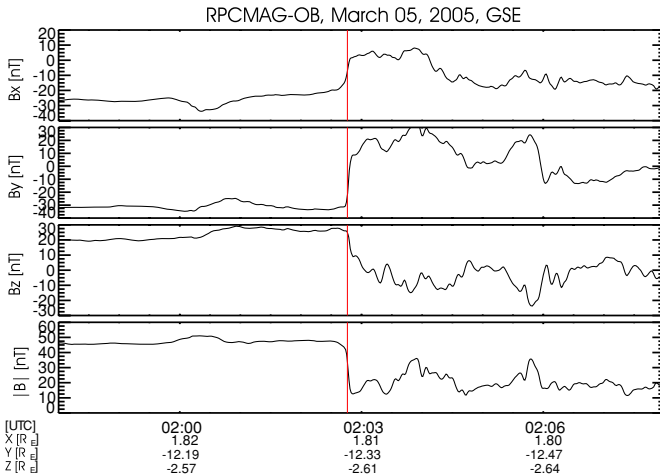

Figure 13. Magnetic field measurements during ROSETTA's outbound Earth magnetopause crossing. The vertical red line indicates the magnetopause crossing.

the traversal took only 6.5 s. A minimum variance analysis identifies the magnetopause normal at $(-0.724, 0.256, 0.640)$ in GSE-coordinates. With this and the known trajectory of ROSETTA a spacecraft seen magnetopause thickness of 21.5 km is determined. This value is rather small compared to typical magnetopause crossings (e.g. Dunlop and Balogh, 2005) and indicates that the magnetopause itself was moving inwards. We summarize that the first scientific observations taken by ROSETTA during its Earth flyby demonstrate that RPC-MAG is a working instrument in space suitable to fulfill the required scientific aims of the ROSETTA Plasma Consortium.

8. Summary

The RPC-MAG magnetic field experiment is a miniaturized, state-of-the-art, triaxial fluxgate magnetometer with two identical sensors mounted inboard and outboard of the 1.5 m long magnetometer boom. Its measurement properties are fully compliant with the measurement requirements specified in the ROSETTA EID-B. After the launch of the ROSETTA spacecraft on March 2, 2004 extensive testing of the functionality of the magnetometer experiment has been performed during several commissioning phases and ROSETTA's first Earth flyby. These tests reveal that the magnetometer experiment is fully functional according its specifications. RPC-MAG is thus ready to perform magnetic field measurements during ROSETTA's visit of comet 67P/Churyumov-Gerasimenko contributing to an increased understanding of the comet-solar wind interaction region and its development during 67P/Churyumov-Gerasimenko's approach to our Sun.

Acknowledgements

References

Acton, C. H.: 1996, *Planet. Space Sci.* **44**, 65.

Alfvén, H.: 1957, *Tellus* **9**, 92.

Auster, U., Apathy, I., Berghofer, G., Remizov, A., Roll, R., Fornacon, K.H., *et al.*: *Space Sci. Rev.*, this issue, doi: 10.1007/s11214-006-9033-x.

Bagdonat, T., Motschmann, U., Glassmeier, K. H., and Kührt, E.: 2004, in Colangeli, L. (ed.), *The New ROSETTA Targets*, Kluwer Academic Publishers, Dordrecht, p. 153.

Balogh, A., Cowley, S. W. H., Dunlop, M. W., Southwood, D. J., Thomlinson, J. G., Glassmeier, K. H., *et al.*: 1993, in *Eur. Space Agency Spec. Publ. No.*, 440.

Baumgärtel, K., Sauer, K., and Bogdanov, A.: 1994, *Science* **263**, 653.

Biermann, L., Brosowski, B., and Schmidt, H. U.: 1967, *Sol. Phys.* **1**, 254.

Blanco-Cano, X., Omidi, N., and Russell, C. T.: 2003, *J. Geophys. Res.* **108**(A5), SSH 11.

Braunbek, W.: 1934, *Zeitschrift für Physik* **59**, 399.

Carr, C., Cupido, E., Lee, C. G. Y., Balogh, A., Beek, T., Dunford, C., *et al.*: RPC – The ROSETTA Plasma Consortium, this issue, doi: 10.1007/s11214-006-9136-4.

Dunlop, M., and Balogh, A.: 2005, *Ann. Geophys.* **23**, 901.

Glassmeier, K. H., and Neubauer, F. M.: 1993, *J. Geophys. Res.* **98**, 20921.

Glassmeier, K. H., Tsurutani, B. T., and Neubauer, F. M.: 1997, in Hada, T. and Matsumoto, H. (eds.), *Nonlinear Waves and Chaos in Space Plasmas*, TERRAPUB, Tokyo, p. 77.

Glassmeier, K. H., Diedrich, A., Richter, I., Eriksson, A., Rother, M., and Milan, S.: 2007, *Planet. Space Sci.*, in preparation.

Hedgecock, P. C. (1975), *Space Sci. Instr.* **1**, 83.

Kertz, W., Lauche, H., and Maier, A.: 1968, Lage und Einrichtung des Magnetischen Laboratoriums des Instituts für Geophysik und Meteorologie, GAMMA 1, Technical University of Braunschweig.

Kügler, H.: 2004a, *Proc. 5th International Symposium on Environmental Testing for Space Programmes*, ESA SP-558, Noordwijk.

Kügler, H.: 2004b, Modell eines Saturationskernmagnetometers basierend auf hochgenauen Kalibriermessungen, Disseration, Technical University of Braunschweig.

Lühr, H.: 1984, MAGNETSRODE: Eine Einrichtung für magnetische Kalibrierungen und Testmessungen, GAMMA 42, Technical University of Braunschweig.

Markgraf, S., Glassmeier, K. H., Musmann, G.: 1996, *IEEE Trans. Geosci. Remote Sens.* **34**, 739.

Maus, S., Rother, M., Holme, R., Lühr, H., Olsen, N., and Haak, V.: 2000, *Geophys. Res. Lett.* **29**, 47.

Maus, S., and Rother, M.: 2004, Potsdam magnetic field model of the Earth, http://www.gfz-potsdam.de/pb2/pb23/SatMag/pomme2.html.

Mehlem, K.: 1978, *IEEE Trans. Magn.* **14**, 1064.

Musmann, G., Neubauer, F. M., Maier, A., and Lammers, E.: 1975, *Raumfahrtforschung* **19**, 232.

Neubauer, F. M., Acuna, M. H., Burlaga, L. F., Franke, B., Gramkow, B., Mariani, F., *et al.*: 1986, in *The GIOTTO Mission and its Science Investigations*, ESA SP-1077, p. 1.

Neubauer, F. M., Glassmeier, K. H., Pohl, M., Raeder, J., Acuna, M. H., Burlaga, L. F., *et al.*: 1986, *Nature* **321**, 352.

Neubauer, F. M.: 1987, *Astron. Astrophys.* **187**, 73.

Neubauer, F. M.: 1991, in Newburn, R. L., *et al.* (eds.), *Comets in the Post-Halley Ery*, Vol. 2, Kluwer Academic, Hingham, Mass, p. 1107.

Ness, N. F., and Donn, B. D.: 1966, *Mem. Soc. R. Liege, Ser.* **5**(12), 141.

Niedner, M. B., and Brandt, J. C.: 1978, *Astrophys. J.* **223**, 655.

Richter, I., Brinza, D. E., Cassel, M., Glassmeier, K. H., Kuhnke, F., Musmann, G., *et al.*: 2001, *Geophys. Res. Lett.* **28**, 1913.

Richter, I., Glassmeier, K. H., Brinza, D. E., Goldstein, R., Henry, M., Musmann, G., *et al.*: 2007, *Planet. Space Sci.*, in preparation.

Russell, C. T., and Huddleston, D. E.: 2000, *Adv. Space Res.* **26**(10), 1665.

Olsen, N., Holme, R., Hulot, G., Sabaka, T., Neubert, T., Tøffner-Clausen, L., *et al.*: 2000, *Geophys. Res. Lett.* **27**, 3607.

Simon, S., Bagdonat, T., Motschmann, U., and Glassmeier, K.H.: 2006, *Ann. Geophys.* **24**, 1.

Slavin, J. A., Goldberg, B. A., Smith, E. J., McComas, D. J., and Bame, S. J.: *Geophys. Res. Lett.* **13**, 1085.

Smith, E. J., Tsurutani, B. T., Slavin, J. A., Jones, D. E., Siscoe, G. L., and Mendis, D. A.: 1986, *Science* **232**, 382.

Sonett, C. P., and Colburn, D. S.: 1968, *Phys. Earth Planet. Interiors* **1**, 326.

Szegö, K., Glassmeier, K. H., *et al.*: 2000, *Space Sci. Rev.* **94**, 429.

Trotignon, J. G., Boström, R., Burch, J. L., Glassmeier, K. H., Lundin, R., Norberg, O., *et al.*: 1999, *Adv. Space Sci.* **24**, 1149.

Tsurutani, B. T., and Smith, E. J.: 1986, *Geophys. Res. Lett.* **13**, 259.

Yumoto, K., Saito, T., and Nakagawa, T.: 1986, *Geophys. Res. Lett.* **13**, 825.